Eur J Med Res (2006) 11: 58-65

Assessment of the Extent of Metastases of Gastrointestinal Carcinoid Tumors Using Whole-body PET, CT, MRI, PET/CT and PET/MRI

M. D. Seemann[1], G. Meisetschlaeger[1], J. Gaa[2], E. J. Rummeny[2]

[1]Department of Nuclear Medicine, [2]Department of Diagnostic Radiology, Technical University, Munich, Germany

Abstract

Objective: To assess the diagnostic value of whole-body positron emission tomography (PET), computed tomography (CT), magnetic resonance imaging (MRI), and the fusion of PET and CT (PET/CT) and PET and MRI (PET/MRI) in the detection of metastatic disease of gastrointestinal carcinoid tumors.

Materials and Methods: This prospective study included six patients with extensive nonresectable metastases of gastrointestinal carcinoid tumors which were consecutively examined from the base of the skull to the proximal thigh using a state-of-the-art PET/CT scanner and a 1.5 Tesla whole-body MRI scanner. PET was performed with a carbohydrated F-18-labeled somatostatin-receptor ligand ([^{18}F]FP-Gluc-TOCA) using a Pico-3D PET scanner. CT was performed with a venous-dominant contrast-enhanced phase using a 16-slice CT scanner. MRI was performed with a coronal T2-weighted Half-Fourier Acquired Single-Shot Turbo Spin Echo (HASTE) sequence, a coronal T2-weighted Turbo-Short Tau Inversion-Recovery (STIR) sequence, a coronal T1-weighted Turbo Spin Echo (TSE) sequence and a high resolution axial T2-weighted TSE sequence. The data sets from PET and CT were fused automatically. The PET and MRI data sets were fused manually. Lesions were rated as metastases if they were not clearly identified as benign lesions according to standard radiological criteria.

Results: For PET, CT, MRI, PET/CT, and PET/MRI, the lesion-by-lesion based analysis showed an overall detection rate for liver metastases (n = 391) of 49.9% (P<.001), 37.1% (*P*<.001), 98.2%, 50.9% (*P*<.001) and 100%, for lymph node metastases (n = 37) of 91.9%, 83.8%, 64.9%, 100% and 97.3% and for osseous metastases (n = 12) of 100%, 8.3% (*P*<.005), 66.7%, 100% and 100%.

Conclusions: PET as single modality revealed the most lymph node and osseous metastases. MRI as single modality revealed the most liver metastases. The combination of molecular/metabolic with anatomical/morphological information improves the diagnostic accuracy for the detection of metastases in comparison to the single modalities. Whole-body PET/MRI is a very promising diagnostic modality for oncological imaging due to the missing radiation exposure and the high soft tissue resolution of MRI in contrast to CT.

Key words: Carcinoid tumors, Whole-body imaging, Positron emission tomography (PET), Computed tomography (CT), Magnetic resonance imaging (MRI), PET/CT, PET/MRI

Introduction

Carcinoid tumors are a heterogeneous group of rare neoplasms of neuroectodermal origin that frequently express specific somatostatin receptors in high densities, which can be of great value in the localization and treatment [12, 21]. The considerable variability in biologic, histological (highly differentiated carcinoid tumors to poorly differentiated neuroendocrine carcinomas), and clinical characteristics [13] are given in various classifications that differ in a number of criteria such as the silver affinity, histological growth pattern, localization of the primary tumor, tumor diameter, metastases, and hormone production [5]. Differentiated endocrine tumors are slow-growing neoplasms, thus permitting long-term survival [13]. These tumors can be clinically symptom free for several years. Metastases can be the first manifestation of the disease, seriously affecting patient prognosis [30]. The complete resection is the only curative therapeutic approach [29]. In an inoperable stage, treatment with a somatostatin analogue (octreotide) is able to control hormone secretion and clinical symptoms in the majority of patients and, in some cases, is able to inhibit tumor growth [16].

Imaging of the whole body to detect gastrointestinal carcinoid tumors and their metastases can be performed by using several different approaches such as somatostatin-receptors using planar scintigraphy, single photon emission computed tomography (SPECT), and positron emission tomography (PET) or morphological changes using computed tomography (CT) and magnetic resonance imaging (MRI). So far, tomographic imaging with radiolabeled analogs of somatostatin (^{111}In-pentetreotide) is accepted as the standard in vivo imaging method in the primary identification and staging of carcinoid and other endocrine tumors. However, there have been great technical improvements in PET, CT and MRI.

We assessed the diagnostic value of the whole-body imaging modalities PET, CT, MRI, and the image fusion of PET and CT (PET/CT) and PET and MRI

(PET/MRI) in the detection of metastases of gastrointestinal carcinoid tumors.

Materials and Methods

Study Patients

In a five-month period, 6 consecutive patients (4 men and 2 woman) suffering from extensive nonresectable metastases of gastrointestinal carcinoid tumor were prospectively examined from the head to the proximal thigh. In all patients, the primary tumor (ileal (n = 3), colonic (n = 2) and appendiceal (n = 1)) was surgically resected several years ago. All imaging procedures of a patient (PET, CT and MRI) were performed in the pretherapeutic tumor staging within 1 week to select those patients who would possibly benefit from a targeted radiolabeled peptide therapy with ^{90}Y-DOTATOC (^{90}Y-[1,4,7,10-tetra-azacyclododecane-N,N^1,N^2,N^3-tetra-acetic acid]^0-Tyr^3-octreotide). All examinations were approved by the local ethics committee. All patients granted informed consent. The mean age ± SD of the patients was 63.3 ± 6.7 years.

Imaging Techniques

Positron-emissions-tomography (PET) data were acquired with a state-of-the-art high-count-rate lutetium oxyorthosilicate (LSO) detector Pico-3D full-ring PET scanner of a PET/CT (biograph Sensation 16®; Siemens AG, Erlangen, Germany). As radiopharmaceutical, a carbohydrated ^{18}F-labeled analogue of octreotide ([^{18}F]FP-Gluc-TOCA = N$^{\alpha}$-(1-deoxy-D-fructosyl)-N$^{\varepsilon}$-(2-[^{18}F]fluoropropionyl)-Lys^0-Tyr^3-octreotate) was used. An activity of 130 ± 20 MBq was intravenously injected 53.3 ± 6.8 minutes before starting the measurements, a time point which has been proven to attain an optimal tumor-to-background ratio. Six to eight bed positions (4 minutes emission per bed position) with a 700-mm field of view (FOV) were measured. Images were reconstructed by means of an iterative procedure (4 iterations) with ordered subsets (8 subsets). Matrix size was 128 x 128.

Computed tomography (CT) data were acquired with a 16-slice CT scanner of the PET/CT. For an optimal assessment of the gastrointestinal tract, oral administration of diluted diatrizoate meglumine (Gastrografin® 1.5%, Schering AG, Berlin, Germany) was performed beginning 1 hour before starting the examination. An anterior-posterior scout-view was obtained for planning and determining the location of the scanning volume. All scans were acquired in a cranio-caudal direction. A venous-dominant contrast-enhanced examination was performed. All patients received a total of 130 ml of a nonionic contrast agent (Imeron® 300, Bracco ALTANA, Pharma GmbH, Konstanz, Germany) infused through an 18-gauge intravenous antecubital catheter using a biphasic contrast-enhanced protocol (85 ml at a flow rate of 3 ml/sec and then 45 mL at 1,8 ml/sec) plus a chaser bolus (30 ml saline with a flow rate of 1.8 ml/sec) by using a dual-head power injector (CT-injector missouri XD 2001®, Ulrich Medical Technic, Ulm, Germany). The examination was started 80 seconds after intravenous contrast media injection. Scanning parameters were 120 kV, 160 mAs, CARE Dose, 16 x 0.75-mm section collimation, 500-msec rotation time, and 15.0-mm table feed per rotation. Images were reconstructed using an increment of 2.5-mm with a 500 mm field of view (FOV) and a kernel of B30f medium smooth. Matrix size was 512 x 512.

Magnetic resonance imaging (MRI) data were acquired with a 1.5 Tesla whole-body MRI scanner (MAGNETOM AVANTO®; Siemens AG, Erlangen, Germany) using the Total Imaging Matrix (TIM) technology [9]. The system is designed for parallel imaging in 3 spatial directions. For the initial whole-body survey sagittal localizers were obtained to set up the plane for the following coronal images that were acquired at five consecutive stations by sequential table movement. On the basis of our experience with this new scanner technology in tumor patients, we decided to perform four different sequences for the assessment of the extent of metastases. First, a coronal T2-weighted Half-Fourier Acquired Single-Shot Turbo Spin Echo (HASTE) sequence was performed (TR = ∞, TE = 118 msec, FA = 150, slice thickness = 6 mm, matrix size 307 x 384, generalized autocalibrating partially parallel acquisition (GRAPPA) 2, TA = 2:45 min). Thereafter, a coronal T1-weighted Turbo Spin Echo (TSE) sequence (TR = 560 msec, TE = 11 msec, FA = 150, slice thickness = 5 mm, matrix size 307 x 384, GRAPPA 2, TA = 13:32 min) and a coronal T2-weighted Turbo-Short Tau Inversion-Recovery (STIR) sequence (TR = 8.020 msec, TE = 73 msec, TI = 150 msec, FA = 150, slice thickness = 5 mm, matrix size 269 x 394, GRAPPA 2, TA = 9:32 min) was performed. To avoid respiratory motion induced artifacts the STIR sequence as well as the T1-weighted TSE sequence in the chest and abdomen were performed with breath-holds. In addition, axial T2-weighted high resolution TSE-sequences (TR = 5.877 msec, TE = 72 msec, FA = 150, slice thickness = 5 mm, matrix size 207 x 384, TA = 3:58 min) using the prospective acquisition with navigator technique (respiratory gating to track diaphragmatic and cardiac movements) were obtained from the chest, abdomen and pelvis. All MRI sequences were performed without application of intravenous or oral contrast media.

Image Interpretation

The PET, CT and MRI examinations were interpreted by a specialist for radiology and nuclear medicine. A diagnosis regarding the presence, the localization and the number of malignant lesions for each patient with respect to organ, lymph node and osseous metastases was performed. The fused images were interpreted using the results from the single modalities. The imaging modality with the most suspicious lesions formed the reference standard.

The axial, coronal and sagittal views of the whole-body PET examinations were interpreted on a standard computer monitor (Viewing Software, Navigator, Siemens AG, Erlangen, Germany). For the evaluation of the PET images standardized uptake values (SUVs) were used as threshold to increase lesion detectability, because of the different physiological tracer uptake in

the liver, spleen and pancreas, and the unspecific tracer accumulation and excretion in the kidneys and the urinary tract (liver: SUV = 12.0; kidney: SUV = 17.0; spleen: SUV = 35.0; soft tissue, lymph nodes and bone: SUV = 5.0). Any focal tracer uptake higher than the choosen SUV for the organ was rated as a pathological tracer accumulation and classified as metastasis.

The axial, coronal and sagittal views of the venous-dominant contrast-enhanced whole-body CT examinations were interpreted on a standard computer monitor (Viewing Software, Navigator, Siemens AG, Erlangen, Germany). For the evaluation of the CT images adapted windows (W) and centers (C) were used to increase lesion detectability (soft tissue: W = 350 and C = 50; lung: W = 1400 and C = -700 and bone: W = 1400 and C = 400).

The axial and coronal views of the whole-body MRI examinations were interpreted on a standard computer monitor (Viewing Software, Navigator, Siemens AG, Erlangen, Germany).

Using CT and MRI, lesions within parenchyma organs were rated as organ metastases if they were not clearly identified as benign lesions (eg, cystic lesions) according to standard criteria (e.g. density and signal intensity). Lymph nodes with a nodular shape and a diameter of more than 10 mm were staged morphologically as lymph node metastases.

The PET and CT data sets were fused automatically (MSViewer®, Navigator, Siemens AG, Erlangen, Germany). The PET and MRI data sets were fused manually using the 3D fusion software of the PET/CT (Navigator, Siemens AG, Erlangen, Germany). Lesions were rated as metastases in the fused images, if they were classified as malignant in at least one of the imaging modalities and certain benign anatomical findings could be excluded.

Statistical Analysis

The exact McNemar test using StatXact® 6 (Cytel Software Corporation, Cambridge, MA, USA) was used to assess the statistical significance in differences in the detection rate of liver, lymph node and osseous metastases for each single procedure and for their combination. All p-values are two-sided. A global significance level of 0.05 was used. Multiple testing was considered using the Bonferroni approach.

Results

In the patients studied we found 391 liver metastases with a size from 2 to 35 mm (Table 1), 37 lymph node metastases with a size from 4 to 30 mm (Table 2 a and b) and 12 osseous metastases with a size from 4 to 14 mm (Table 3).

Table 1. Lesion-by-lesion based overall detection rate for liver metastases.

	Number of lesions	%	Significance level
PET	195	49.9	P < 0.001
CT	145	37.1	P < 0.001
MRI	384	98.2	P = 0.83
PET/CT	199	50.9	P < 0.001
PET/MRI	391	100	*reference standard*

Table 2a. Lesion-by-lesion based overall detection rate for lymph node metastases.

	Number of lesions	%	Significance level
PET	34	91.9	P = 0.81
CT	31	83.8	P = 0.54
MRI	24	64.9	P = 0.12
PET/CT	37	100	reference standard
PET/MRI	36	97.3	P = 0.92

Table 2b. Lesion-by-lesion based overall detection rate for lymph node metastases in different topographical localizations.

	cervical	mediastinal	hilar	retroperitoneal	intraperitoneal
PET	4 (100)	6 (100)	1 (100)	11 (91.7)	12 (85.7)
CT	3 (75.0)	4 (66.7)	1 (100)	10 (83.3)	13 (92.9)
MRI	3 (75.0)	4 (66.7)	1 (100)	7 (58.3)	9 (64.3)
PET/CT	4 (100)	6 (100)	1 (100)	12 (100)	14 (100)
PET/MRI	4 (100)	6 (100)	1 (100)	12 (100)	13 (92.9)

Note. Values are number of lesions. Values in parenthese are percentages.

Table 3. Lesion-by-lesion based overall detection rate for osseous metastases.

	Number of lesions	%	Significance level
PET	12	100	reference standard
CT	1	8.3	P < 0.005
MRI	8	66.7	P = 0.12
PET/CT	12	100	reference standard
PET/MRI	12	100	reference standard

For the detection of liver metastasis, PET/MRI (n = 391; 100%) and MRI (n = 384; 98.2%) were most sensitive, whereas PET/CT (n = 199; 50.9%) (*P*<.001), PET (n = 195; 49.9%)(*P*<.001) and CT (n = 145; 37.1%)(P<.001) were significantly less reliable. MRI showed a lot of lesions with a diameter between 2 and 4 mm which could not be seen in any other modality (Fig. 1). Nevertheless, in one patient we found in the combination with PET 7 more lesions, because of problems with the navigator technique in the MRI.

For the detection of lymph node metastases, PET/CT (n = 37; 100%), PET/MRI (n = 36; 97.3%) and PET (n = 34; 91.9%) were most sensitive, whereas CT (n = 31; 83.8%)(P<.54) and MRI (n = 24; 64.9%)(P<.12) were considerably less reliable. 6 lymph nodes (16.2%) (cervical n = 1, mediastinal n = 2, retroperitoneal n = 2 and intraperitoneal n = 1) showed a clearly increased tracer uptake in the PET but were smaller than 10 mm in the CT (Fig. 2). 3 lymph nodes (n = 8.1%) (retroperitoneal n = 1 and intraperitoneal n = 2) showed a size from 11 to 14 mm in the CT but no increased tracer uptake in the PET. Using MRI, abdominal lymph node metastases were difficult to differentiate from small and large intestine.

For the detection of osseous metastases, PET (n = 12; 100%), PET/CT (n = 12; 100%) and PET/MRI (n = 12; 100%) were most sensitive, whereas MRI (n = 8; 66.7%)(P<.12) and CT (n = 1; 8.3%)(P<.003) were less reliable. The missing osseous metastases in the MRI were localized in the ribs. The metastasis seen on CT was osteosclerotic.

The cardiac metastasis with a size of 15 mm was seen on PET, PET/CT and PET/MRI and the intrapulmonary metastasis with a size of 11 mm was seen on PET, CT, PET/CT and PET/MRI.

Discussion

In our study, MRI was the most sensitive imaging procedure in the detection of liver metastases. The main reason is the spatial resolution in the submillimeter area and the high soft tissue contrast. PET, CT and PET/CT underestimated the extension of liver metastases or even missed the metastatic disease, because of the low soft tissue contrast in CT and the low spatial resolution and physiological tracer uptake in the PET. Nevertheless, PET seems to be able to give additional information to MRI if there are problems with the navigator technique. PET was the most sensitive imaging procedure in the detection of lymph node metastases. The main advantage of lymph node staging with PET is the sensitive detection of serotonin-expressing small lymph nodes (<10 mm) which are not assessable with morphologic imaging and can be identified leading to an improvement of the reference standard. The detection rate of 100% for lymph node staging in the combination of PET and morphologic imaging is not a realistic value, because it is possible that individual lymph node metastases showed no octreotate accumulation and also were not enlarged. PET was also the most sensitive imaging procedure in the detection of osseous metastases. Schillaci et al. [22] compared the detection of abdominal metastasis in SRS SPECT and conventional imaging procedures (ultrasound, CT and/or MRI) in carcinoid tumors. In agreement to our results, they suggested that only the combined use of molecular and morphological imaging procedures achieved a correct classification. Antoch et al. [1] compared FDG-PET/CT and MRI in patients with different malignant diseases. They suggested the use of FDG-PET/CT as a possible first line modality for whole-body tumor staging. However, they did not perform an image fusion of PET and MRI. Our result suggested, that the combination of PET and MRI could be a very valuable whole-body diagnostic imaging tool not only for carcinoid tumors, but also for oncological tumor staging.

In the literature, somatostatin-receptor imaging (^{111}In-pentetreotide SPECT) using somatostatin analogue as radiotracer has proven to be the most important diagnostic procedure for a correct classification of primary carcinoid tumors and in identifying of metastases and thus, the most reliable tool for guiding therapy [10, 15, 17, 22-24]. In contrast to conventional imaging procedures (specificity, 85.7%), neither SRS SPECT nor planar scintigraphy showed false-positive results in differentiating liver metastases from small-size hemangiomas (specificity, 100%) [24]. Nevertheless, the limited sensitivity of SRS SPECT is a problem of the high variance in the expression of somatostatin-receptors among the different tumor entities and even within different lesions in single patients [7, 11, 19, 21], the limitations of the physical properties of gamma camera imaging with planar images and SPECT and due to the pharmacokinetic characteristics of ^{111}In-octreotide with high physiological uptake in liver, spleen and kidney and elimination at a varying percentage by the hepatobiliary system. Tumors can be cached due to a low target to background ratio and by the markedly bowel activity in the images. To reduce the limitations of somatostatin-receptor scintigraphy, we used the imaging method with the highest resolution, the positron emissions tomography (PET) and a

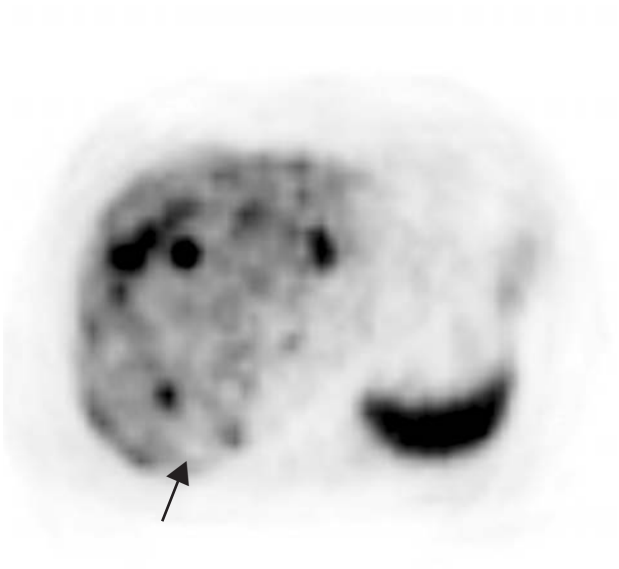

a

b

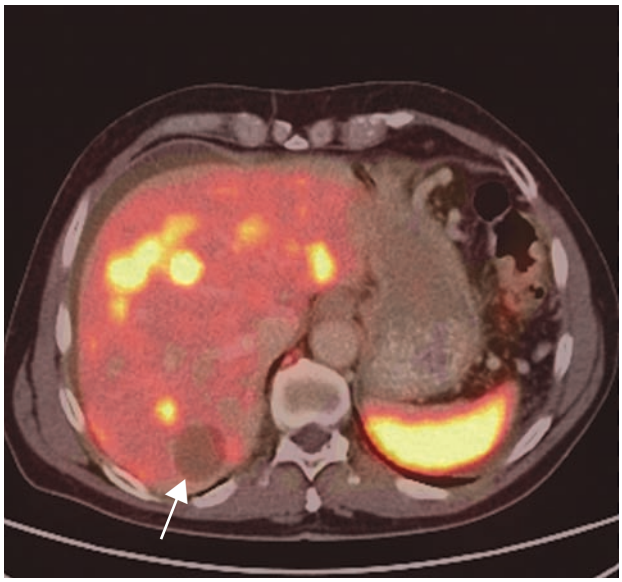

c

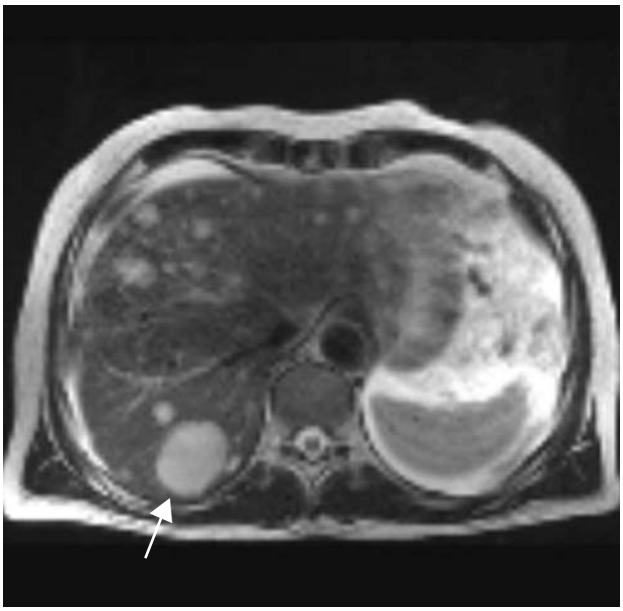

d

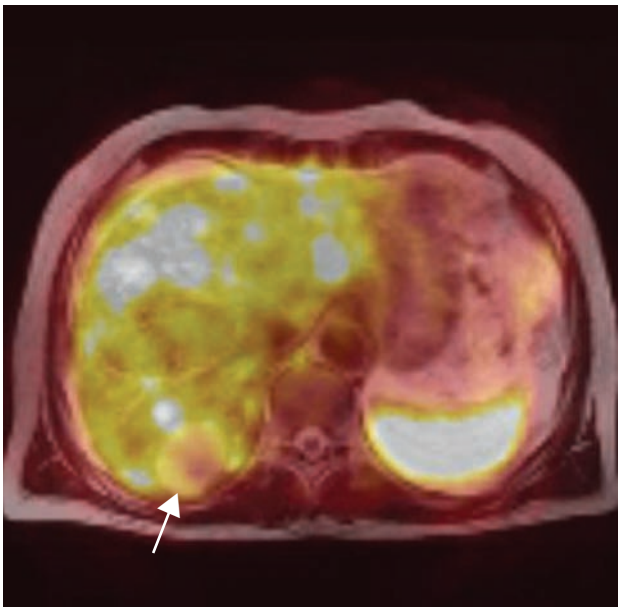

e

Fig. 1. 71-year-old male patient with an extensive metastatic disease of an intestinal carcinoid tumor. Corresponding axial view from the epigastric region showing a [^{18}F]FP-Gluc-TOCA PET image (a), a venous-dominant contrast-enhanced CT image (b), an automatic fused image of PET and CT (PET/CT) (c), a T2-weighted TSE image of MRI (d), and a manual fused image of PET and MRI (PET/MRI) (e) with multiple hepatic metastases. PET, CT and the overall view of all MRI sequences identified a great cyst in the right lobe of the liver (arrow). Furthermore, CT and MRI revealed a peri-hepatic and peri-splenic fluid colletion, because of peritoneal extension of the disease.

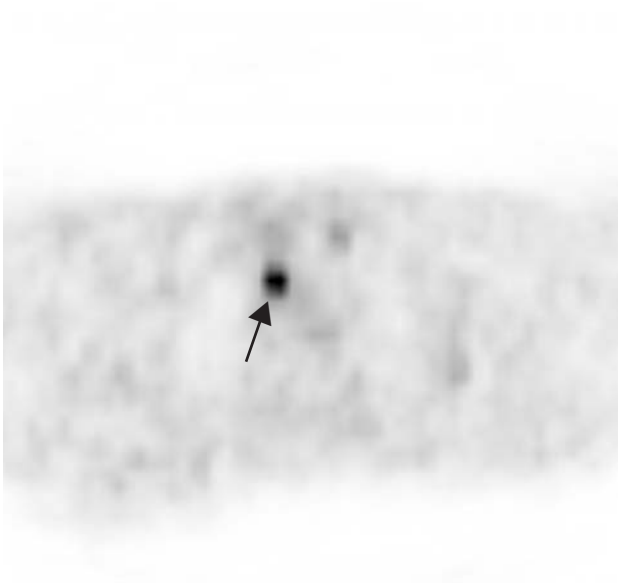

a

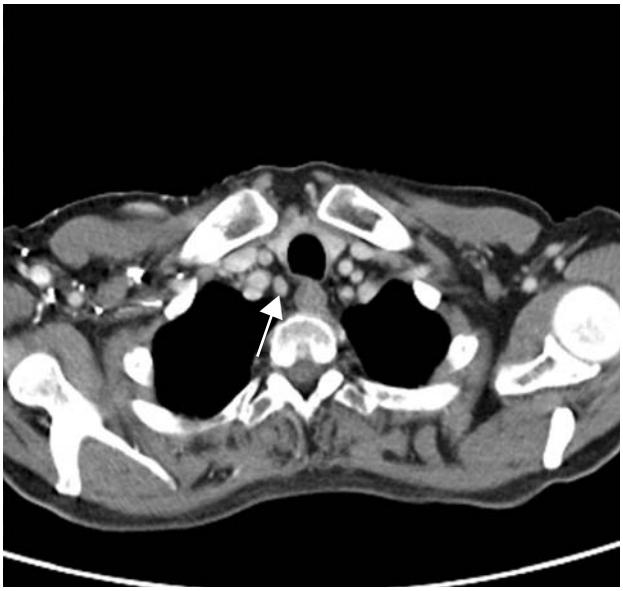

b

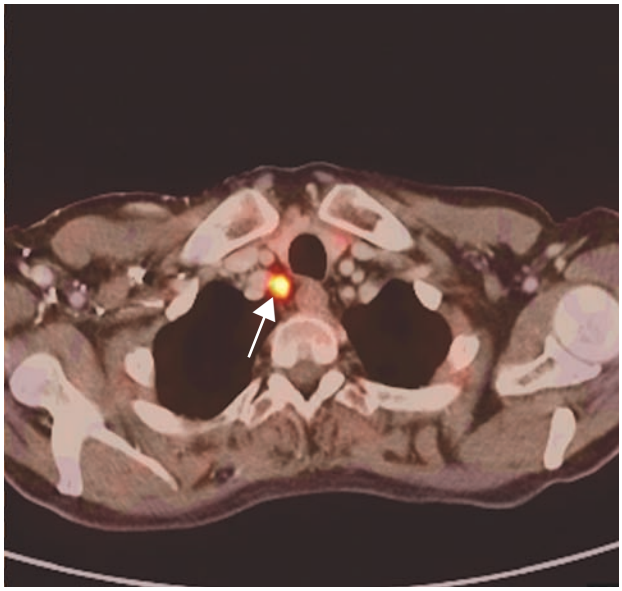

c

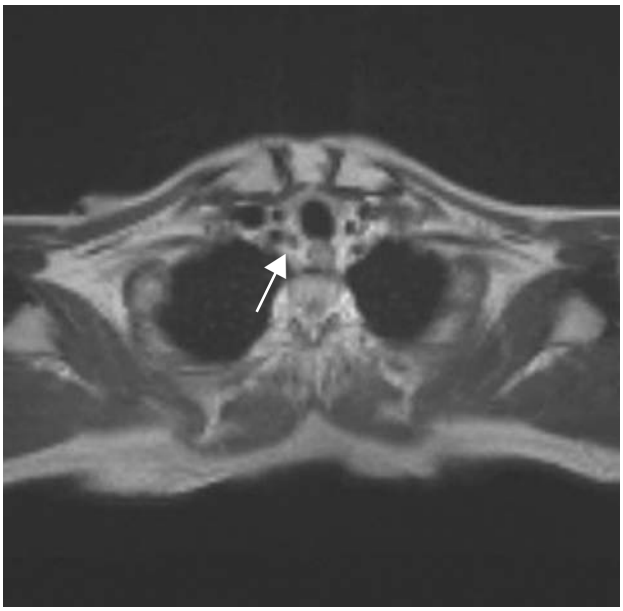

d

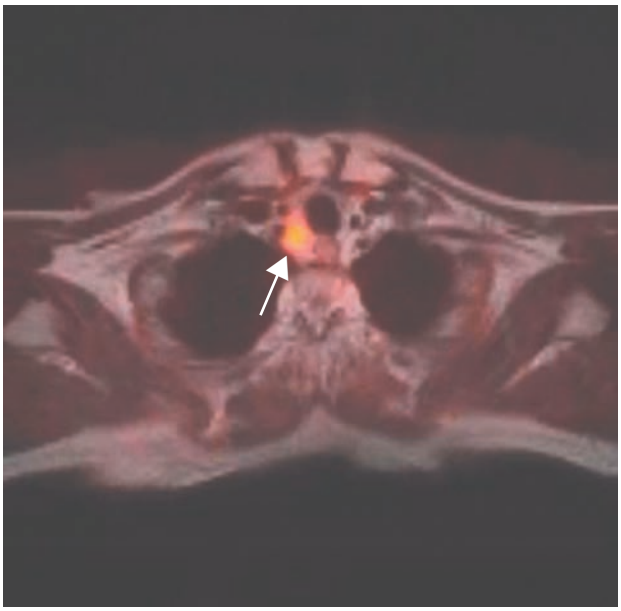

e

Fig. 2. 62-year-old male patient with an extensive metastatic disease of an intestinal carcinoid tumor. Corresponding axial view from the inlet of the thorax showing a [^{18}F]FP-Gluc-TOCA PET image (a), a venous-dominant contrast-enhanced CT image (b), an automatic fused image of PET and CT (PET/CT) (c), a T2-weighted TSE image of MRI (d), and a manual fused image of PET and MRI (PET/MRI) (e). PET identified a small lymph node metastasis (5 x 6 x 8 mm) (arrow).

carbohydrated F-18-labeled somatostatin-receptor ligand. The preclinical evaluation of [^{18}F]FP-Gluc-TOCA (N^{α}-(1-deoxy-D-fructosyl)-N^{ε}-(2-[^{18}F]fluoropropionyl)-Lys^{0}-Tyr^{3}-octreotate) showed a high affinity to human somatostatin-receptor (hsst) 2, a moderate affinity to hsst 5, a low affinity to hsst 4 and no affinity to hsst 1 and 3. Furthermore, [^{18}F]FP-Gluc-TOCA is characterized by a low lipophilicity. Its rapid renal elimination, low liver uptake and low intestinal activity as well as its fast and high tumor accumulation provides excellent tumor to non tumor ratios [31].

Over the past decade major improvements in CT and MR imaging have occured. The advent of multidetector CT (MDCT) and the increase of detectors allowed further improvements in image resolution. The ability to reconstruct images with a very thin slice thickness improves the resolution and allows the creation of high resolution reformatted images in any anatomical plane. The improvements in the hardware of MRI machines facilitates the development of fast and ultrafast pulse sequences as well as the development of phased-array multicoils allowing for higher signal to noise ratio and thus higher anatomic resolution. In addition, the advent to navigator techniques further enhances signal to noise ratio and spatial resolution due to multiple signal avering allowing for higher imaging matrices, resulting in improved diagnostic performance in the detection of liver lesions [18]. However, one potential drawback (eg, image blurring) of this technique might occur if the navigator is incorrectly placed or the patient has an irregularly breathing pattern. Then, the navigator technique should be replaced by fast or ultra fast breath-hold techniques [8] avoiding respiratory or motion induced artifacts. However, breath-hold techniques suffer from poorer signal to noise ratio and limited spatial resolution (eg, image matrix 256 vs 384 or 512 using navigators). The weakness of lymph node staging is the known lack of reliable criteria, since assessment can be made only on the basis of size [4]. Furthermore, the differentiation of abdominal lymph nodes and small intestine without contrast media, the detection of osseous metastases in the ribs and the differentiation of degenerative changes of the vertebral column and bone metastases could be a problem. Therefore, the whole-body CT and MRI protocols have to be optimized to allow a better differentiation of abdominal lymph nodes and small intestine and osseous metastases.

Our results support the introduction of whole-body PET/MRI as new diagnostic modality. Nevertheless, our study is limited in certain respects. First of all, the number of patients examined is relatively small and does not allow a satisfying statistical analysis. Performing CT with a venous-dominant contrast-enhanced phase and MRI without the use of an intravenous paramagnetic contrast medium may include the possibility of overlooking some hypervascular metastases that can only be seen in the hepatic arterial-dominant contrast-enhanced phase [2, 6, 20]. However, Dromain et al. [6] found no significant difference between the hepatic arterial-dominant contrast-enhanced T1-weighted images and the fast spin-echo T2-weighted images in the detection of hepatic metastases from carcinoid tumors. The fast spin-echo T2-weighted sequence showed a significantly higher lesion-to-liver contrast-to-noise ratio than the hepatic arterial-dominant contrast-enhanced T1-weighted sequence. Although primary disease of carcinoid tumor was proven in all patients, a detailed lesion-by-lesion histopathologic analysis was not possible because most of the patients in this series had an extensive metastatic disease and therefore did not undergo a further resection.

Conclusions

Whole-body imaging allows the evaluation both the region of the primary tumor and the presence of metastases at the same time. PET facilitates the evaluation of molecular aspects and metabolic alterations that are fundamental in the detection of malignancies, assessment of tumor stage, therapeutical response and tumor recurrence. The main advantage of PET is its high sensitivity in identifying of cancerous areas at an early stage. In generally, the accelerated radiotracer activity can be seen before anatomical structure changes. The main difficulty with PET is the lack of an anatomical reference frame. CT and MRI are excellent morphological imaging modalities. Whole-body CT and MRI produce large amounts of image data, resulting in the possibility of overlooking subtle pathological findings. The combination of PET with CT or MRI can compensate for their disadvantages and therefore offers several advantages in comparison to PET and CT and MRI alone. In scientific literature, the fusion of molecular/metabolic with anatomic/morphologic information has been shown to improve the diagnostic accuracy for staging of cancer and to allow discrimination of variable physiologic radiotracer uptake that can mimic metastatic lesions [3, 14, 25, 28]. Although PET/CT has shown its clinical value it might not be the ultimate diagnostic goal since MRI offers several advantages as compared with CT. The results of our study suggested that the combination of PET and MRI improves the diagnostic accuracy in the assessment of the extent of metastatic disease of gastrointestinal carcinoid tumors. The combination of whole-body PET and MRI into a single scanner is a very promising diagnostic modality for oncological imaging due to the missing radiation exposure and the high soft tissue resolution of MRI in contrast to CT [26, 27].

References

1. Antoch G, Vogt FM, Freudenberg LS, Nazaradeh F, Goehde SC, Barkhausen J, Dahmen G, Bockisch A, Debatin JF, Ruehm SG (2003) Whole-body dual-modality PET/CT and whole-body MRI for tumor staging in oncology. JAMA 290: 3199-3206
2. Bader TR, Semelka RC, Chiu VC, Armao DM, Woosley JT (2001) MRI of carcinoid tumors: spectrum of appearances in the gastrointestinal tract and liver. J Magn Reson Imaging 14: 261-269
3. Blomqvist L, Torkzad MR (2003) Whole-body imaging with MRI or PET/CT: the future for single-modality imaging in oncology? JAMA 290: 3248-3249
4. Bollen EC, Goei R, van´t Hof-Grootenboer BE, Versteege CW, Engelshove HA, Lamers RJ (1994) Interob-

server variability and accuracy of computed tomographic assessment of nodal status in lung cancer. Ann Thorac Surg 58: 158-162
5. Capella C, Heitz PU, Hoefler H, Solcia E, Kloeppel G (1994) Revised classification of neuroendocrine tumors of the lung, pancreas and gut. Digestion 55: 11-23
6. Dromain C, de Baere T, Baudin E, Galline J, Ducreux M, Boige V, Duvillard P, Laplanche A, Caillet H, Lasser P, Schlumberger M, Sigal R (2003) MR Imaging of hepatic metastases caused by neuroendocrine tumors: comparing four techniques. AJR 180: 121-128
7. Fujita T, Yamaji Y, Sato M, Murao K, Takehara J (1994) Gene expression of somatostatin receptor subtypes, SSTR1 and SSTR2, in human lung cancer cell lines. Life Sci 55: 1797-1806
8. Gaa J, Fischer H, Laub G, Georgi M (1996) Breath-hold MR imaging of focal liver lesions: comparison of fast and ultrafast techniques. Eur Radiol 6: 838-843
9. Gaa J, Rummeny EJ, Seemann MD (2004) Whole-body imaging with PET/MRI. Eur J Med Res 9: 309-312
10. Gibril F, Reynolds JC, Doppmann JL, Chen CC, Venzon DJ, Termanini B, Weber HC, Stewart CA, Jensen RT (1996) Somatostatin receptor scintigraphy: its sensitivity compared with that of other imaging methods in detecting primary and metastatic gastrinomas. Ann Intern Med 125: 26-34
11. Hofland LJ, Lamberts SW (2001) Somatostatin receptor subtype expression in human tumors. Ann Oncol 12 (Suppl 2): 31-36
12. Kaltsas G, Rockall A, Papadogias D, Reznek R, Grossman AB (2004) Recent advances in radiological und radionuclide imaging and therapy of neuroendocrine tumours. Eur J Endocrinol 151: 15-27
13. Kloeppel G, Heitz PU, Capella C, Solcia E (1996) Pathology and nomenclature of human gastrointestinal neuroendocrine (carcinoid) tumors and related lesions. World J Surg 20: 132-141
14. Kluetz PG, Meltzer CC, Villemagne VL, Kinahan PE, Chander S, Martinelli MA, Townsend DW (2000) Combined PET/CT imaging in oncology: impact on patient management. Clin Pos Imag 3: 223-230
15. Krenning EP, Kwekkeboom DJ, Bakker WH, Breeman WA, Kooij PP, Oei HY, van Hagen M, Postema PT, de Jong M, Reubi JC, et al. (1993) Somatostatin receptor scintigraphy with [^{111}In-DTPA-D-Phe1]- and [123I-Tyr3]-octreotide: the Rotterdam experience with more than 1000 patients. Eur J Nucl Med 20: 716-731
16. Kvols LK, Moertel CG, O´Connel MJ, Schutt AJ, Rubin J, Hahn RG (1986) Treatment of the malignant carcinoid syndrome: evaluation of a long-acting somatostatin analogue. N Engl J Med 315: 663-666
17. Lamberts SWJ, Krenning EP, Reubi JC (1991) The role of somatostatin and its analogs in the diagnosis and treatment of tumors. Endocr Rev 12: 430-482
18. Martin DR, Semelka RC (2001) Imaging of benign and malignant focal liver lesions. Magn Reson Imaging Clin N AM 9: 785-802
19. Patel YC (1999) Somatostatin and its receptor family. Front Neuroendocrinol 20: 157-198
20. Paulson EK, McDermott VG, Keogan MT, DeLong DM, Frederick MG, Nelson RC (1998) Carcinoid metastases to the liver: role of triple-phase helical CT. Radiology 206: 143-150
21. Reubi JC, Kvols LK, Waser B, Nagomey DM, Heitz PU, Charboneau JW, Reading CC, Moertel C (1990) Detection of somatostatin receptors in surgical and percutaneous needle biopsy samples of carcinoids and islet cell carcinomas. Cancer Res 50: 569-577
22. Schillaci O, Scopinaro F, Angeletti S, Tavolaro R, Danieli R, Annibale B, Gualdi G, Delle Fave G (1996) SPECT improves accuracy of somatostatin receptor scintigraphy in abdominal carcinoid tumors. J Nucl Med 37: 1452-1456
23. Schillaci O, Annibale B, Scopinaro F, Delle Fave GF, Centi Colella A (1997) Somatostatin receptor scintigraphy of malignant somatostatinoma with indium-^{111}-pentetreotide. J Nucl Med 38: 886-887
24. Schillaci O, Spanu A, Scopinaro F, Falchi A, Danieli R, Marongiu P, Pisu N, Madeddu G, Delle Fave G, Madeddu G (2003) Somatostatin receptor scintigraphy in liver metastasis detection from gastroenteropancreatic neuroendocrine tumors. J Nucl Med 44: 359-368
25. Seemann MD (2004) PET/CT: fundamental principles. Eur J Med Res 9: 241-246
26. Seemann MD (2005) Whole-body PET/MRI: the future in oncological imaging. Technol Cancer Res Treat 4: 577-582
27. Seemann MD, Gaa J (2005) Images in cardiovascular medicine. Cardiac metastasis: visualization with positron emission tomography, computed tomography, magnetic resonance imaging, positron emission tomography/computed tomography, and positron emission tomography/magnetic resonance imaging. Circulation 112: e329-330
28. Shreve PD, Anzai Y, Wahl RL (1999) Pitfalls in oncologic diagnosis with FDG PET imaging: physiologic and benign variants. Radiographics 19: 61-77
29. Stinner B, Kisker O, Zielke A, Rothmund M (1996) Surgical management for carcinoid tumors of small bowel, appendix, colon and rectum. World J Surg 20: 183-188
30. Sutliff VE, Doppman JL, Gibril F, Venzon DJ, Yu F, Serrano J, Jensen RT (1997) Growth of newly diagnosed, untreated metastatic gastrinomas and predictors of growth patterns. J Clin Oncol 15: 2420-2431
31. Wester H.-J., Schottelius M., Scheidhauer K, Meisetschlaeger G, Herz M, Rau FC, Reubi JC, Schwaiger M (2003) PET imaging of somatostatin receptors: design, synthesis and preclinical evaluation of a novel ^{18}F-labelled, carbohydrated analogue of octreotide. Eur J Nucl Med Mol Imaging 30: 117-122

Received: December 20, 2005 / Accepted: January 9, 2006

Address for correspondence:
Marcus D. Seemann, M.D.
Associate Professor of Radiology
Department of Nuclear Medicine
Technical University, Munich
Ismaninger Strasse 22
D-81675 Munich, Germany
Tel. ++49 89 4140 2971
Fax ++49 89 4140 4841
e-mail: m.seemann@lrz.tum.de